

Merging of Super-Alfvénic Current Filaments during Collisionless Weibel Instability of Relativistic Electron Beams

Oleg Polomarov,¹ Igor Kaganovich,² and Gennady Shvets¹

¹*Department of Physics and Institute for Fusion Studies, The University of Texas at Austin, Austin, Texas 78712, USA*

²*Plasma Physics Laboratory, Princeton University, Princeton, New Jersey 08543, USA*

(Received 31 October 2007; published 20 October 2008)

The theoretical framework predicting the long-term evolution, structure, and coalescence energetics of current filaments during the Weibel instability of an electron beam in a collisionless plasma is developed. We emphasize the nonlinear stage of the instability, during which the beam density of filaments increases to the background ion density, and the ambient plasma electrons are fully expelled from the filaments. Our analytic and numerical results demonstrate that the beam filaments can carry super-Alfvénic currents and develop hollow-current density profiles. This explains why the initially increasing magnetic field energy eventually decreases during the late stage of the instability.

DOI: 10.1103/PhysRevLett.101.175001

PACS numbers: 52.40.Mj, 52.35.Qz, 52.65.-y

The electromagnetic Weibel instability (WI) of plasmas with anisotropic velocity distribution is one of the most basic and long-studied collective plasma processes [1–5]. The dynamics and energetics of its nonlinear saturation are important for both laboratory and astrophysical plasmas. The WI is likely to play an important role in the fast ignitor scenario [6] because it can result in the collective energy loss of a relativistic electron beam in a target plasma [6–13]. Collisionless WI has been suggested [14–18] as a mechanism for relativistic collisionless shock formation in gamma ray bursts. Shock dynamics depends on the long-term evolution of the magnetic field. Specifically, it is not clear whether the long-term magnetic fields generated during the coalescence of current filaments remain finite [9] or decay with time [16] (and if they do, according to what physical mechanism). In this Letter we elucidate such mechanism and relate it to the merger of filaments bearing super-Alfvénic current ($I > I_A = \gamma\beta mc^3/e$, see, e.g., [19]) during the late stage of the WI.

We develop a physical model describing the structure and coalescence energetics of the beam and return current filaments produced as a result of the WI of an electron beam in the collisionless background plasma. For tractability, the analytic model is 2D in cylindrical geometry, whereas the supporting particle-in-cell (PIC) simulations are 2D in space (corresponding to a very long electron beam pulse propagating in the homogeneous z direction) and 3D in the plasma and beam momenta [20]. We identify three qualitatively different stages of the WI, as illustrated by Fig. 1: (i) the linear stage resulting in formation of filaments and exponential growth of the magnetic field that saturates due to magnetic trapping of the beam particles [3,4], (ii) the nonlinear stage corresponding to the merger of sub-Alfvénic ($I < I_A$) beam filaments and *increase* of the magnetic field energy that saturates when the filaments' beam current reaches approximately I_A [5,14], and (iii) the highly nonlinear stage, corresponding to the merger of super-Alfvénic ($I > I_A$) filaments and *decreas-*

ing magnetic field energy. The filaments with hollow beam current density structure similar to the Hammer-Rostoker equilibrium [19,21] with the outer return current develop and coalesce during stage (iii). In this Letter we emphasize this least-studied stage of the WI. We analytically predict that the magnetic energy decreases when super-Alfvénic filaments coalesce, thereby explaining the magnetic field decay during the late stages of WI [9].

During the extensively studied [3–5,9,12,14,17] stage (i) of the WI, the electron beam of initial density $n_{b0} < n_0$ and radius $R_{\text{init}} \gg c/\omega_{pe}$ breaks up into a large number of filaments of the typical radius $\sim c/2\omega_{pe}$, where c is the speed of light, $\omega_{pe} = \sqrt{4\pi e^2 n_0/m}$ is the electron plasma frequency, and n_0 is the initial uniform ion density (ions are treated as infinitely massive, see also [22]). The end of stage (i) [“knee” in the growth rate of magnetic energy shown in Fig. 1(b)] corresponds to the saturation of WI due to magnetic trapping of the beam electrons [3,4]. During the linear stage [12], instability grows with the exponen-

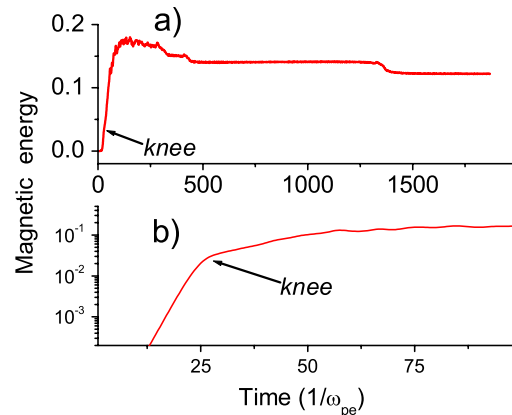


FIG. 1 (color online). PIC simulations of the dynamics of the magnetic field energy: (a) long-term evolution, (b) short-time zoom-in. The magnetic field energy is normalized to the initial beam energy.

tiation rate $\gamma \sim \omega_{pe} \sqrt{n_b/n_0}$, corresponding to the filamentation regime [23] of the Weibel instability. The nonlinear stage (ii) corresponds to the merger of these filaments occurring on a time scale longer than ω_{pe}^{-1} . Therefore, quasineutrality of the beam-plasma system ($n_b + n_e \approx n_0$) is approximately maintained as confirmed by PIC simulations [12]. During stage (ii) of the filaments' merger their density increases until the background plasma electrons are expelled from the filament: $n_b \approx n_0$ (if initially $n_b/n_0 \geq 0.05$). Therefore, our analytic model addresses the merger of the filaments with fully expelled plasma electrons from their interior ($n_b = n_0$) surrounded by the return current of the ambient plasma during the nonlinear stages (ii) and (iii). In analyzing the merger of two filaments with the initial beam radii R_0 and currents I_0 into a single filament of beam radius $R_1 = \sqrt{2}R_0$ (which follows from conservation of particles for the cylindrical beams with $n_b = n_0$) and current I_1 , we pose and will answer the following question: What is the change of the magnetic energy $\Delta U_B \equiv U_{B1} - 2U_{B0}$ and filament current $\Delta I \equiv I_1 - 2I_0$ as the result of the merger?

We start by estimating the magnetic energy of a single evacuated cylindrical beam filament with the beam density $n_b = n_0$ for $r < R$ and $n_b = 0$ for $r > R$. The beam filament is surrounded by the return current of the ambient plasma with density $n_e = n_0$ for $r > R$ and $n_e = 0$ for $r < R$. The dominant electromagnetic field is the in-plane magnetic field $\vec{B}_\perp = -\vec{e}_z \times \vec{\nabla} \psi$ [8,12,13], where $\vec{A}_z \equiv \vec{e}_z \psi$ is the vector potential. We assume that the initial electron beam with the forward momentum $\vec{P} = \vec{e}_z p_{b0}$ is underdense with respect to the quiescent ambient plasma: $n_{b0} < n_0$. The following normalized quantities are used below: $\tilde{x} = \omega_{pe} x/c$, $\tilde{t} = \omega_{pe} t$, $\tilde{n} = n/n_0$, $\beta_{e,bz} = v_{e,bz}/c$, $\tilde{p}_{e,bz} = p_{e,bz}/mc$, $\tilde{\psi} = e\psi/mc^2$, $\vec{B} = eB/mc\omega_{pe}$, and $\vec{E} = eE/mc\omega_{pe}$. Tildes are dropped in what follows. Using conservation of the longitudinal canonical momentum, fluid momenta of the beam and the plasma in the filament are given by $p_{bz}(r) = p_{b0} + \psi(r)$ and $p_{ez} = \psi(r)$ [12]. For the case of nonrelativistic beam and plasma, Ampere's law for the inner or outer parts of the filament can be expressed as $\nabla^2 \psi = n_e(r)\beta_{ez} + n_b(r)\beta_{bz}$. For filaments with expelled plasma electrons it yields $\nabla^2 \psi - \psi = \theta(r)\beta_{b0}$, where $\theta(r < R) = 1$ and $\theta(r > R) = 0$. Requiring the continuity of ψ and $B_\theta = \partial_r \psi$ at $r = R$ and solving the above equation results in the analytic expressions for the beam's and the plasma's axial velocities:

$$\beta_{bz}(r) = \beta_{b0} I_0(r) K_1(R) R, \quad \beta_{ez}(r) = -\beta_{b0} K_0(r) I_1(R) R. \quad (1)$$

These are plotted in the top row of Fig. 2 for thin ($R = 0.5$) and thick ($R = 4$) filaments. It is apparent that the beam velocity is strongly peaked at the filament's periphery whenever $R \gg 1$. The resulting hollow-current distribu-

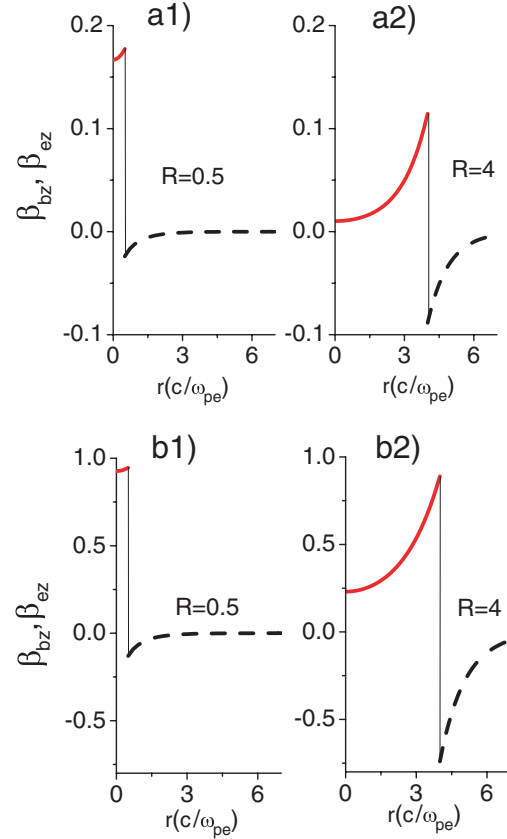


FIG. 2 (color online). Normalized velocities β_{bz} and β_{ez} of the beam (solid red line) and plasma (dashed black line) for $R = 0.5$ (a1),(b1), $R = 4$ (a2),(b2). Top: The nonrelativistic case (a1),(a2) with $\beta_{bz0} = 0.2$. Bottom: The relativistic case (b1),(b2) with $\beta_{bz0} = 0.95$.

tion for the beam part of the filament corresponds to the classic Hammer-Rostoker [19,21] equilibrium of a charge-neutralized beam with a flattop density distribution. Note that an electron beam filament with $R \gg 1$ carries a super-Alfvénic current: $I_b/I_A^0 = R I_1(R) K_1(R) R/2$, where $I_A^0 = \beta_{b0} mc^3/e$. For $R \gg 1$ this expression is simplified to $I_b/I_A^0 \approx R/4 > 1$, while for $R \ll 1$ we find that $I_b/I_A^0 \approx R^2/4 \ll 1$. Note that the beam and plasma velocities as well as the filaments' beam current (equal by construction to the plasma return current) and the magnetic energy are parametrized by only two parameters: the initial beam velocity β_{b0} and the filament's radius R . These quantities are calculated for *two* noninteracting filaments of radius R_0 before merger and *one* resulting (coalesced) filament with radius $R_1 = \sqrt{2}R_0$. Normalized beam current and filament magnetic field energy are expressed as $\bar{I}_b(R) = 2 \int_0^R dr r \beta_{bz} / \beta_{b0} R^2$ and $\bar{U}_B(R) = \int_0^\infty dr r |\partial_r \psi|^2 / R^2$. The initial (premerger) current and energy are given, respectively, by $2\bar{I}_b(R_0)$ and $2\bar{U}_B(R_0)$. The same post-merger quantities are given by $\bar{I}_b(R_1)$ and $\bar{U}_B(R_1)$. Both premerger (black curves) and postmerger [gray (red) curves] quantities are plotted in Fig. 3 (top). Independently of the fila-

ments' radius R_0 , the total current of the merged filament is decreased during the merger; see Fig. 3(a2) and 4. The beam longitudinal momentum changes due to inductive electric field caused by alternating magnetic field in going from one equilibrium to another. Remarkably, the total magnetic energy can either increase (for $R < R_{\text{crit}} \approx 1.5$) or decrease (for $R > R_{\text{crit}}$) as the result of the merger, as shown in Fig. 3(a1) and in Figs. 1 and 4. Qualitatively, the merger of two small sub-Alfvénic beam filaments results in addition of the single filament currents: $\bar{I}_b(R_1) \approx 2\bar{I}_b(R_0)$. This is because for $R < 1$, the filament's current is uniformly distributed across the entire filament and is therefore approximately proportional to its area. Correspondingly, the total magnetic field energy approximately doubles as the result of the merger. The situation drastically changes for wide super-Alfvénic filaments: the beam current is concentrated within the skin depth c/ω_{pe} of its periphery. The peripheral region of large filaments decreases by a factor $\sim\sqrt{2}$ compared with two smaller filaments before merger. Therefore, the total current of the merged filaments decreases by a factor $\sim\sqrt{2}$ and, consequently, the total magnetic field energy decreases approximately by the same factor during the merger. The transition from magnetic energy growth to decay is clearly seen in Fig. 1. The underlying mechanism is the continuous

expansion in size of the beam filaments. As soon as the filaments' size exceeds R_{crit} the magnetic field energy starts decreasing after the filaments' merger. Note that from the standpoints of a two-fluid (beam and plasma) electron MHD the change in magnetic flux associated with the filaments is due to the generation of the vorticity of the beam current density (i.e., $\vec{\nabla} \times \vec{j}_b$).

We proceed by considering coalescence of two relativistic beam filaments. For analytic tractability, we consider the merger of two identical magnetically self-confined filaments with the beam particles in Hammer-Rostoker equilibrium [19,21]. Namely, all beam electrons are assumed to have the same relativistic energy $\gamma_j = \gamma$ and longitudinal canonical momentum $\gamma_j \beta_{jz} - \psi(\vec{x}_{\perp j}) \approx p_{b0}$. Ambient plasma electrons (return current) are treated as a cold nonrelativistic fluid with $\beta_{ez} = \psi$. Ampere's law for this case gives $\nabla^2 \psi = [1 - \theta(r)]\psi + \gamma^{-1}\theta(r)[\psi + p_{b0}]$. This equation is solved requiring that (a) $\psi = 0$ for $r = \infty$, (b) ψ and $\partial\psi/\partial r$ are continuous at the beam edge $r = R$, and (c) beam particles turn around at the beam edge: $\gamma^2 = 1 + [p_{b0} + \psi(R)]^2$. Condition (c) enables relating γ to the beam radius R and the initial (prefilamentation) beam momentum p_{b0} . Therefore, as in the nonrelativistic case, both the beam filaments' current and magnetic field are determined by just two parameters: the beam radius R and the beam initial (prefilamentation) relativistic momentum p_{b0} . The analytic solutions are

$$\beta_{bz}(r) = \frac{\beta_{bR}}{I_0 \left[\frac{R}{\sqrt{\gamma}} \right]} I_0 \left[\frac{r}{\sqrt{\gamma}} \right], \quad \beta_{ez}(r) = \frac{\beta_{pR}}{K_0(R)} K_0(r), \quad (2)$$

where constants β_{bR} , β_{eR} , and γ are found from conditions (a)–(c) resulting in the system of transcendental equations that was numerically solved. Beam and plasma electron velocity profiles are plotted in Fig. 2 (bottom panel) for narrow [Fig. 2(b1): $R = 0.5$, $\gamma = 3.08$] and wide [Fig. 2(b2): $R = 4$, $\gamma = 2.18$] filaments with $\beta_{b0} = 0.95$.

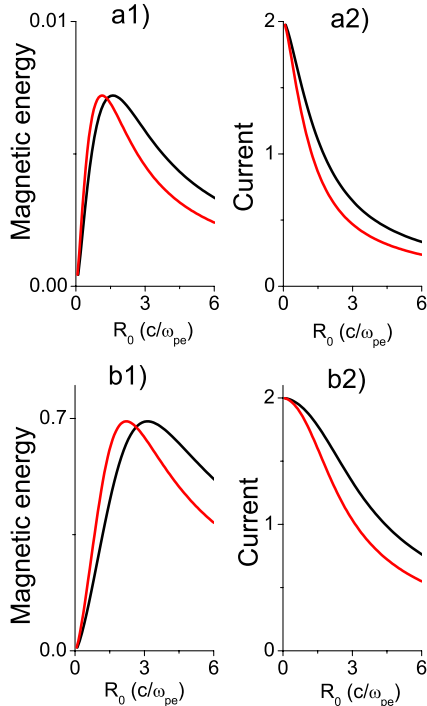


FIG. 3 (color online). Normalized magnetic energy $2\bar{U}_B(R_0)$ (a1),(b1) and normalized current $2\bar{I}_b(R_0)$ (a2),(b2) for two filaments (black line) with radii R_0 , and $\bar{U}_B(R_1)$ and $\bar{I}_b(R_1)$ for one filament [gray (red) line] with $R_1 = \sqrt{2}R_0$. Top: (a1), (a2) corresponding to $\beta_{bz0} = 0.2$. Bottom: (b1), (b2) corresponding to $\beta_{bz0} = 0.95$.

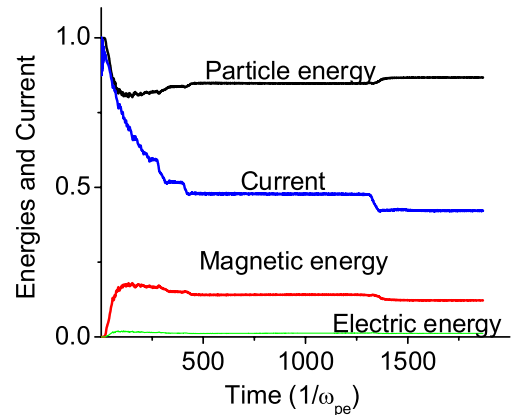


FIG. 4 (color online). PIC-simulated normalized magnetic (red line), particle (black line), electric (green line) energies, and normalized (to its initial value) current (blue line) corresponding to parameters of Fig. 1.

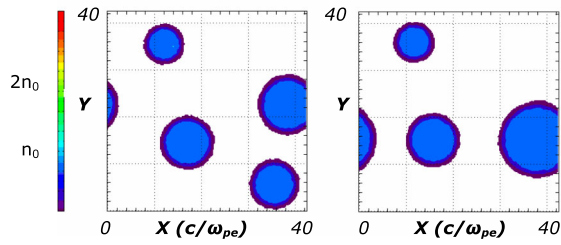


FIG. 5 (color online). PIC-simulated beam density for $\omega_{pe}t = 1300$ (left) and for $\omega_{pe}t = 1600$ (right). Parameters the same as in Figs. 1 and 4.

Just as in the nonrelativistic case, we consider the energetics of the coalescence of two relativistic filaments with the radii R_0 and relativistic energy per particle $\gamma_0 mc^2$ into a single relativistic filament with radius $R_1 = \sqrt{2}R_0$ and per-particle energy $\gamma_1 mc^2$. The previously defined normalized beam current $\bar{I}_b(R)$ and magnetic energy $\bar{U}_B(R)$ are plotted in Fig. 3 (bottom panel) for two filaments with R_0 (black line) and a single merged filament with R_1 [gray (red) line]. As in the nonrelativistic case, coalescence of small filaments ($R < R_{\text{crit}} \approx 3$) leads to the magnetic energy increase, while the merger of large filaments ($R > R_{\text{crit}} \approx 3$) reduces the magnetic energy, as shown in Fig. 3(b1).

To confirm the analytic predictions, full PIC simulations of the filaments' merger have been carried out using the LSP code [24]. The starting point of the simulations is a spatially uniform cold electron beam with $n_{b0}/n_0 = 0.2$ and $\beta_{b0} = 0.95$ which is charge and current neutralized by the ambient plasma. Periodic conditions are applied at the boundaries of the $40c/\omega_{pe} \times 40c/\omega_{pe}$ simulation domain. The total beam current is $I_{0b} \approx 8I_A$. The simulation results shown in Fig. 1 indeed confirm that the magnetic energy growth during stage (ii) (small filaments' merger) gives way to magnetic energy decline during stage (iii) (large filaments' merger). The smooth decline of U_B at the start of stage (iii) ($t \approx 200/\omega_{pe}$) is due to the presence of a large number of high-current filament pairs undergoing simultaneous coalescence. As the number of filaments becomes smaller, their mergers become pairwise events clearly separated in time. This is reflected in the stepwise changes of the beam current and the magnetic or particle energies shown in Fig. 4. The largest stepwise magnetic energy decline shown in Fig. 4 occurs at $t \approx 1400/\omega_{pe}$ due to the merger of two super-Alfvénic hollow-current filaments. Two snapshots of this merger are shown in Fig. 5. The two merging beam filaments initially carry $I_1 \sim 2.65I_A$ and $I_2 \sim 2.41I_A$ while the resulting filament carries $I \sim 4.46I_A < I_1 + I_2$. Density profiles of the merging beam filaments shown in Fig. 5 indicate that the ambient plasma

electrons are indeed fully expelled from the beams' interior, with the narrow ion sheaths surrounding them. The electric field energy localized in the sheath is negligible compared with the magnetic energy as shown in Fig. 4.

In conclusion, we have developed a robust analytical model describing the energetics of merging of the sub- or super-Alfvénic flattop and hollow-current density filaments in the ambient plasma. Our model predicts, and PIC simulations confirm, that such mergers are responsible for the magnetic energy decay during the late stages of the Weibel instability.

This work was supported by the U.S. DOE Grant No. DE-FG02-05ER54840. We thank E. Startsev, A. Pukhov, A. Spitkovsky, U. Keshet, and S. Kalmykov for fruitful discussions.

-
- [1] E. W. Weibel, Phys. Rev. Lett. **2**, 83 (1959).
 - [2] B. D. Fried, Phys. Fluids **2**, 337 (1959).
 - [3] R. L. Morse and C. W. Nielson, Phys. Fluids **14**, 830 (1971).
 - [4] R. C. Davidson *et al.*, Phys. Fluids **15**, 317 (1972).
 - [5] R. Lee and M. Lampe, Phys. Rev. Lett. **31**, 1390 (1973).
 - [6] M. Tabak *et al.*, Phys. Plasmas **1**, 1626 (1994).
 - [7] J. J. Honrubia and J. Meyer-ter-Vehn, Nucl. Fusion **46**, L25 (2006).
 - [8] T. Taguchi *et al.*, Phys. Rev. Lett. **86**, 5055 (2001).
 - [9] L. O. Silva *et al.*, Phys. Plasmas **10**, 1979 (2003).
 - [10] V. M. Malkin and N. J. Fisch, Phys. Rev. Lett. **89**, 125004 (2002).
 - [11] J. M. Hill *et al.*, Phys. Plasmas **12**, 082304 (2005).
 - [12] O. Polomarov *et al.*, Phys. Plasmas **14**, 043103 (2007).
 - [13] M. Honda *et al.*, Phys. Rev. Lett. **85**, 2128 (2000).
 - [14] M. V. Medvedev and A. Loeb, Astrophys. J. **526**, 697 (1999).
 - [15] M. V. Medvedev *et al.*, Astrophys. J. **618**, L75 (2005).
 - [16] A. Gruzinov, Astrophys. J. **563**, L15 (2001).
 - [17] L. O. Silva *et al.*, Phys. Plasmas **9**, 2458 (2002).
 - [18] A. Spitkovsky, Astrophys. J. Lett. **673**, L39 (2008).
 - [19] R. C. Davidson, *Physics of Nonneutral Plasmas* (Addison-Wesley, Reading, MA, 1990), p. 122.
 - [20] If the beam length is less than the ion skin depth then our 2D slice model can describe the 3D case; see I. Kaganovich *et al.*, Phys. Plasmas **8**, 4180 (2001).
 - [21] D. A. Hammer and N. Rostoker, Phys. Fluids **13**, 1831 (1970).
 - [22] The finite ion mass can lead to modification of ion density profiles and expulsion of plasma from the filaments' edges by the radial electric field. Nevertheless, the qualitative features of the magnetic field dynamics and filaments' structure remain similar.
 - [23] A. Bret *et al.*, Phys. Rev. Lett. **94**, 115002 (2005).
 - [24] Simulations were performed with LSP PIC code which is a product of ATK Mission Research, Albuquerque, NM 87110, U.S.A.